"Equatorial Small-Angle X-Ray Scattering Study of Porosity and Pore-Size Distribution in Polyester and Their Influence on Dyeing Behavior"

A. K. KULSHRESHTHA,* M. V. S. RAO,† and N. E. DWELTZ,
Ahmedabad Textile Industry's Research Association,
Ahmedabad - 380 015, India

Synopsis

For explaining the dyeing behavior of polyester (PET) fibers, the important role played by pores has been speculated upon in modern dyeing theories. In the present work, an attempt has been made to characterize the pore size spectrum in morphologically very different PET fibers by means of equatorial small-angle X-ray Scattering (SAXS). The analysis of the scattering curves reveals that all the samples analyzed in the present work have a two-phase structure, consisting of pores of widely different sizes dispersed within a matrix of the polymer network. This polydispersity of pore sizes is revealed from Guinier plots, as well as from an analysis of intensities in the tail of the scattering curves, which are found to obey Porod's Law. Estimates have been made of pore radii, pore concentration in the substrate, and specific surface. The pore size distribution function has been obtained using a new procedure. Various parameters of the pore size spectrum are discussed in relation to the morphological structure of fibers, as well as their significance to dyeing. The diffusion behavior of solvent molecules within PET is also discussed.

INTRODUCTION

The problem of relating the dyeing behavior of polyethylene terephthalate (PET) fibers to their morphology has presented some kind of enigma and evaded a plausible solution. The uptake of disperse dyes by polyester follows a complex behavior[1]—it first decreases as the setting temperature is raised, but increases again at higher temperatures until it equals, or exceeds, that of the untreated control. Since the degree of crystallinity (DC) improves continuously with increasing temperature, it is perplexing to see an increase in dye uptake (DU) at higher temperatures of setting. Changes in DU are believed to occur due to changes in fiber morphology during manufacture and subsequent stages of textile processing (melt spinning, drawing, crimping/texturing, spinning, weaving, setting, dyeing and allied processes). Measurements of morphological parameters (moisture regain, density, orientation, DC, crystallite size and its distribution and perfection) show that variations in DU cannot be explained by a fringed-micellar model of fiber structure. This is understandable because these parameters do not characterize the order-disorder situation within noncrystalline regions where dye diffusion is presumed to occur. The present state of the dyeing

* Present address: R & D Division, Indian Petrochemicals Corporation, Ltd., Baroda - 391 346, India.
† Present address: Man Made Textiles Research Association, Surat - 395 002, India.

Journal of Applied Polymer Science, Vol. 30, 3423–3443 (1985)
 CCC 0021-8995/85/083423-20$04.00

theory is not satisfactory because it does not tell the dyer which parameters to control. As a result, dyeing still remains an art.

Studies of PET fiber morphology in relation to its dyeing[1-5] have proved to be valuable since they point out the need to look a little closer at the noncrystalline regions within the PET substrate and in particular at the distribution of "nonmatter" or voids (which we shall call a "pore" for convenience) within the noncrystalline regions. There has been some ambiguity since a large number of synomymous terms have been used in literature to describe the nonmatter, for example, micropores, microvoids, microcavities, microdefects, microcracks, microheterogeneities, holes, sites, channels, internal space, accessible space, spaces between the morphological units, free volume, noncrystalline volume (created by segregation between crystalline and noncrystalline zones), etc. The nomenclature and use of the term "pore" for describing nonmatter is convenient because the resultant fiber property can be called porosity. Pores within fibers, which can conceivably be created by segmental mobility or by removal of low-molecular-weight oligomers, provide space for dye penetration, its transport through the fiber structure and its final accommodation. A relatively small increase in the molecular size of the diffusing species requires a disproportionately large increase both in the pore volume necessary for diffusion, as well as the activation energy of diffusion. Fiber porosity can thus be a measure of the accessibility of the fiber to disperse dye particles.

It is possible to visualize the PET fiber as a two-phase system formed by the distribution of nonmatter (i.e., pores) within matter (composed of an entire spectrum of order ranging from crystalline through paracrystalline to amorphous states). The theory of small-angle X-ray scattering (SAXS) by two-phase systems has been considerably developed.[6-9] SAXS not only facilities verification of the two-phase hypothesis, but also permits a determination to be made of pore sizes, their concentration, as well as the specific surface area, all these being characteristic properties of the distribution of nonmatter within a fiber matrix. Equatorial SAXS studies have been made on natural fibers (cellulose,[10] sisal,[11] agave cantala,[12] agave hybrid,[13] kangaroo tail tendon,[14] elastoidin[15]) and synthetic fibers (aramid fibers[16] and carbon fibers from pitch and lignin[17]). No such work is available on PET.

The present work was undertaken with a view to study the porosity and pore size distribution within PET fibers by means of SAXS. Several PET fibers were selected, covering a wide spectrum of structural differences. The uptake of disperse dye (DU) and solvent diffusion behavior of these substrates were determined in order to relate the dye uptake with fiber porosity on the one hand and van der Waals diameter of the diffusing species on the other. The results obtained suggest that pore volume is one of the dominant structural parameters affecting the uptake of disperse dyes by PET.

EXPERIMENTAL

Materials

Present investigations were conducted on the following PET fibers which were deliberately modified to have a wide spectrum of structural differences:

Sample 1: Melt-spun, as extruded PET tow (noncrystalline, unoriented).

Sample 2: Sample 1 cold-drawn at room temperature to 400% extension (noncrystalline, oriented).

Sample 3: Sample 1 isothermally crystallized at 200°C (crystalline, unoriented).

Sample 4: Sample 2, isothermally crystallized under tension (not allowed to shrink) at 200°C (crystalline, oriented).

Small Angle X-Ray Scattering

Equatorial distributions of continuous SAXS from PET fibers were measured with a slit-collimated Kratky low-angle X-ray diffractometer, using CuKα radiation which was monochromated by a nickel filter in the primary beam. The intensity of the scattered beam was measured in the fixed-counts mode by a scintillation counter coupled with a pulse height discriminator which improves monochromatization. Fibers were mounted in the sample holder with their lengths parallel to the slits. Intensities were measured by moving the counter stepwise through the scattering range (1.5 mrad to 40 mrad) by lifting the vacuum chamber by means of a precision spindle. At least 3200 pulses were counted at each counter position. Up to $2\theta = 10$ milliradians, the number of pulses was usually at least 12,800.

Optimum scanning conditions (entrance slit width = 100 μm, counter slit width = 250 μm, counter slit length = 20mm) were determined by varying slit openings of incident beam and counter. An X-ray beam was produced whose width at half intensity was 1.45 mrad and whose height was effectively infinite. The primary beam intensity was constant along its length. The SAXS limit of resolution was between 800 and 1000 Å, depending upon the magnitude of the scattered intensity. Absolute intensity and scattering power of the primary beam was evaluated using the Lupolen calibration standard supplied with the Kratky apparatus. Scattered intensities were corrected for background and absorption effects.[10,18] In our experimental setup, the sample-to-receiving-slit distance, a, was equal to 205 mm.

Dyeing

Different PET samples were dyed in a dye bath maintained at 90 $\pm$ 2°C using C.I. Disperse Blue 7 dye (without carrier). The amount of dye taken up by fibers was estimated using well-known methods.[19,20]

Solvent Diffusion Behavior

Solvent diffusion behavior of PET samples was examined using a phenol/tetrachloroethane mixture as a solvent and the criticial dissolution times (CDT) were measured in seconds using a known method.[21]

Morphological Parameters

Structural data on PET samples were obtained from density, birefringence, sonic modulus, X-ray diffraction and infrared measurements, employing standard procedures.[22,23]

ANALYSIS OF SAXS DATA

Analysis of the Initial Portion of the Scattering Curve (Guinier's Method)

Assuming a spherical shape for the pores, SAXS intensity at small 2θ is given by Guinier's approximation[24]:

$$I(2\theta) = I(\theta) \exp\left[-(4\pi^2/5\lambda^2)\, R_E^2\, (2\theta)^2\right] \tag{1}$$

where 2θ is the scattering angle, $I(2\theta)$ is the scattered intensity at 2θ, λ is the wavelength of X-rays, and R_E is the Guinier radius (pore size). For scattering angles in the SAXS region,

$$2\theta = \tan 2\theta = X/a \tag{2}$$

where a is the sample-to-receiving-slit distance and X is the linear distance of the receiving slit from the centroid of the beam in the plane perpendicular to a.

The Guinier plots are obtained by plotting ln I vs. $(2\theta)^2$. The slope of the initial linear region in the Guinier plot is given by

$$\text{slope} = -(4\pi^2/5\lambda^2)\, R_E^2 \tag{1'}$$

from which R_E can be determined.

Analysis of the Tails of the Scattering Curve (Porod's Method)

The technique most free from assumptions concerning the sample and one that is applicable to the present experimental arrangement is that due to Porod, in which the tails of the experimental scattering curve are examined to locate a region for which $\lim[X^3 I(X)]$ may be determined. Some portion of the scattering curve must have a significant range for which the product $X^3 I(X)$ remains constant. This arises from the fact that for a two-phase structure the tail of the smeared curve should obey the relation[6,7]

$$I(X) \propto 1/X^3 \tag{3}$$

or

$$X^3 I(X) = K$$

where K is the characteristic constant. By plotting I vs. X^{-3}, the above relation can be experimentally verified. Alternatively, a plot of log I vs. log X should have a linear region of slope (-3).

Pore Radius

For a polydisperse system of particles [obeying eq. (3)], the average pore radius P is given, according to Porod,[6] by

$$P = \frac{3a\lambda}{8\pi} \int_0^\infty \frac{XI(X)dX}{(1 - C)X^3 I(X)} \tag{4}$$

$$= \frac{3a\lambda}{8\pi(1 - C)} \frac{Q_{\text{exp}}}{K} \tag{4'}$$

where

$$Q_{\text{exp}} = \int_0^\infty XI(X)dX \tag{5}$$

is called the invariant of the scattering curve and C is the volume fraction of pores (scattering entities). Q_{exp} depends upon the scattering power of the scatterers and is independent of their size and shape.

Specific Surface Area

The specific surface area of the sample, S_{sp}, is a function of[6,25] the characteristics constant K, the invariant Q_{exp}, and the volume fraction of the scattering pores C in the sample

$$S_{\text{sp}} = \frac{S}{V} = \frac{8\pi C(1 - C)K}{\lambda a Q_{\text{exp}}} \tag{6}$$

Specific surface area S_{sp} has units of cm^2/cm^3 and is the ratio of the total surface area S of the scattering pores to the sample volume V.

Length of Coherence

According to Porod,[6] the length of coherence l_c is given by

$$l_c = \frac{a\lambda E}{2Q_{\text{exp}}} \tag{7}$$

where

$$E = \int_0^\infty I(X)dx \tag{8}$$

is the integrated scattered energy.

Range of Inhomogeneity

The range of inhomogeneity l_r is given by[26]

$$l_r = \frac{4C}{S_{\text{sp}}} \tag{9}$$

where l_r represents the average transmission path through the pores (also called the "transversal length").

Determination of C

Theoretical value of the invariant is given by[10]

$$Q_{th} = 16.68 \times 10^{-3} \times P_s \times t \times a \times \rho^2 \times C \times (1 - C) \tag{10}$$

where t is the sample thickness, ρ is the electron density of the PET matrix, and P_s is the primary beam energy weakened by the scattering sample. Determination of P_s is carried out with the help of a calibration standard (Lupolen), according to a procedure outlined by Kratky, Pilz, and Schmitz. The electron density of PET is given by the relation

$$\rho = d \cdot \frac{\Sigma A}{\Sigma W}$$

where d is the apparent density of the PET sample, ΣA is the sum of atomic numbers, and ΣW is the sum of the atomic weights in the repeat unit of PET. Since C is very small, eq. (10) becomes

$$Q_{th} = 16.68 \times 10^{-3} \times P_s \times t \times a \times \rho^2 \times C \tag{11}$$

Comparing the theoretical and experimental values of the invariant and rearranging, the volume fraction of the pores is obtained in terms of the experimentally obtained values:

$$C = \frac{Q_{exp}}{16.68 \times 10^{-3} \times P_s \times t \times a \times \rho^2} \tag{12}$$

Determination of Pore-Size Distribution

A practical procedure has been developed by Harkness, Gould, and Hren[27] (hereafter abbreviated HGH) in which only spherical scatterers (pores) having a log normal size distribution (LND) function are assumed for the exact evaluation of any experimental SAXS curve. The HGH analysis using LND applies only when the Porod approximation holds [i.e., $X^3\, I(X)$ becomes constant over an interval]. The assumption of the log normal distribution has been justified[27,28] by its wide range of application and its ability to adequately describe the size distributions that arise from nucleation, growth, and coarsening processes. Basically, the assumption implies that the rate of growth decreases as pores (scatterers) become large. Size distributions determined using the HGH procedure are in excellent agreement[27,28] with the size distributions obtained using electronmicroscopy.

The distribution of pore radii is given[29] by

$$F(R) = (R\sqrt{2\pi} \cdot \ln \sigma)^{-1} \exp\left\{-\left[\frac{(\ln R - \ln \mu^2)}{2 \ln^2 \sigma}\right]\right\} \tag{13}$$

where

$$\ln \mu = \ln R_E - 1.71 \ln(R_E/P) \tag{14}$$

and

$$\ln^2 \sigma = (1/3.5) \ln (R_E/P) \tag{15}$$

The constant μ and σ characterize the log normal distribution of eq. (13). SAXS data gives information regarding ratios of various moments[21] of $F(R)$, for instance,

$$R_E^2 = \langle R^7 \rangle / \langle R^5 \rangle \tag{16}$$

and

$$P = \langle R^3 \rangle / \langle R^2 \rangle \tag{17}$$

RESULTS AND DISCUSSION

Small-Angle X-Ray Scattering

The Guinier plots for various PET samples are shown in Figure 1. The Guinier approixmation, i.e., the linearity of the plot, is valid only for small values of $(2\theta)^2$. At large $(2\theta)^2$, data points curve away from the straight line, indicating a breakdown of the asymptotic form of eq. (1). A curved Guinier plot, as is presently the case, indicates that there is a considerable nonuniformity of pore sizes. The absence of a maximum in Figure 1 also indicates a nonuniformity of pore sizes and a randomness in their distribution. The average pore sizes R_E for different PET fibers have been estimated from the slope of the initial linear portions of the Guinier plot and are listed in Table I.

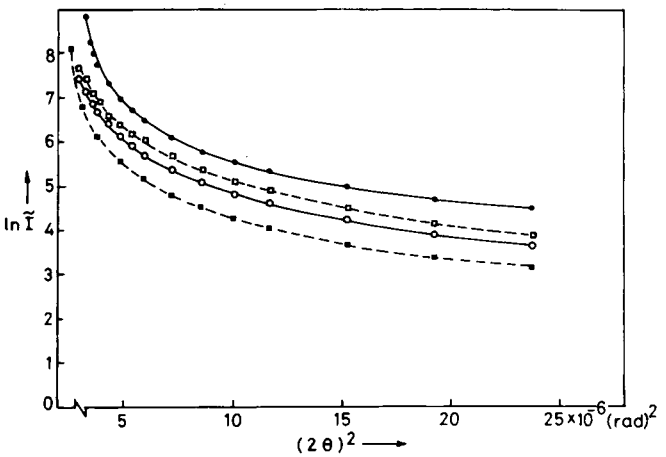

Fig. 1. Guinier plots for Polyester: (- - ○ -) Undrawn tow; (●) Undrawn tow tension-quenched; (- - □ -) Tow drawn 400%; (■) Drawn tow tension-quenched.

TABLE I
SAXS Parameters of Various PET Samples

SAXS parameter \ Sample	Sample 1, as-spun tow	Sample 2, tow drawn 400%	Sample 3, as-spun tow, tension-quenched at 200°C	Sample 4, drawn tow, tension-quenched at 200°C
Guinier pore size R_E (Å)	480	460	810	520
Porod pore size P (Å)	210	205	760	220
Length of coherence, l_c (Å)	635	650	825	630
Range of inhomogeneity l_r (Å)	275	270	1020	290
Volume fraction of pores, C (%)	0.04	0.04	0.16	0.02
Specific surface S_{sp} (m^2/cm^3)	0.062	0.062	0.061	0.025
Q_{exp} (mm^2)	198	253	1456	116
E (mm)	797	1040	7607	461
P_s	1.92×10^6	1.84×10^6	1.62×10^6	1.82×10^6
μ (Å)	114	114	725	119
σ (Å)	1.63	1.62	1.14	1.64

The double log plots (Fig. 2) for all PET samples have linear regions of slope ≈ -3, indicating that the substrates are polydisperse, have a two-phase structure and that the scattered intensities vary according to Porod's law. A plot of X^3I vs. X^3 is shown in Figure 3. From the linear regions, the characteristic constant K has been evaluated, which gives the limiting value of X^3I.

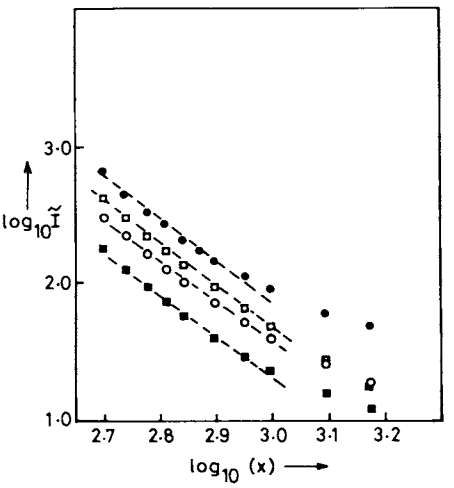

Fig. 2. Log plots of small-angle data: (○) Undrawn tow; (●) Undrawn tow tension-quenched; (□) Tow drawn 400%; (■) Drawn tow tension-quenched.

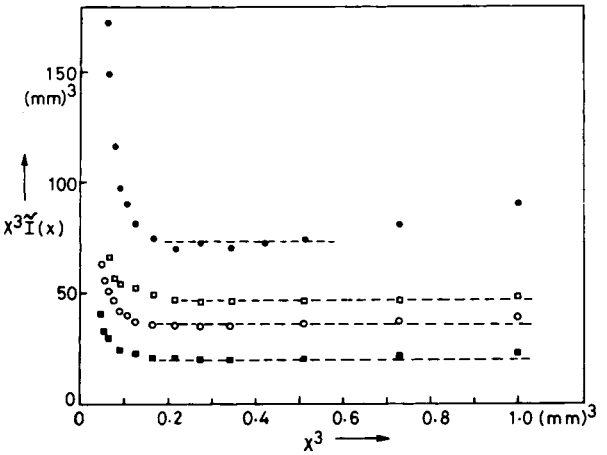

Fig. 3. Small-angle X-ray scattering from polyester: (○) Undrawn tow; (●) Undrawn tow tension-quenched; (□) Tow drawn 400%; (■) Drawn tow tension-quenched.

The concentration (i.e., the volume fraction) of pores C in different PET samples has been evaluated from the experimentally determined values using eq. (12). Using the volume fraction C, the characteristic constant K, and the invariant Q_{exp}, the pore size according to Porod, P, the specific surface area S_{sp}, the length of coherence l_c, and the range of inhomogenity l_r have been calculated using eqs. (4)–(9). All these SAXS parameters, as well as related experimental values, are listed in Table I. The distribution functions for different PET samples obtained by the HGH procedure[27,28] [i.e., eqs. (13)–(15)] are compared in Figures 4(a)–4(d), where the fraction of pores, $F(R)$, is plotted as a function of their spherical radii size R. From an examination of these curves, the following facts emerge: (i) Cold-drawing does not produce any change in the pore size spectrum of polyester [Fig. 4(a)]. This perhaps can be explained as due to the plastic nature of defor-

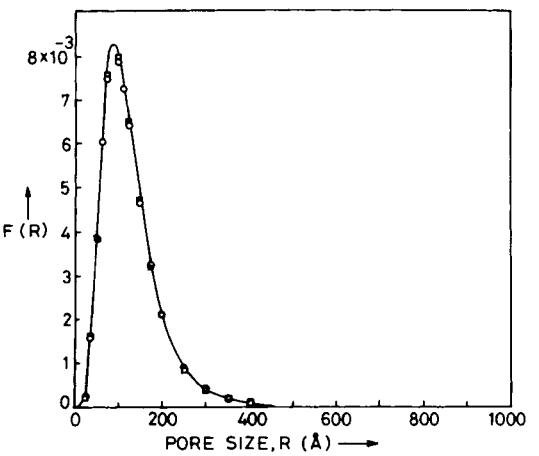

Fig. 4(a). Pore-size distribution in noncrystalline polyester: (○) as-spun Tow; (□) Tow drawn 400%.

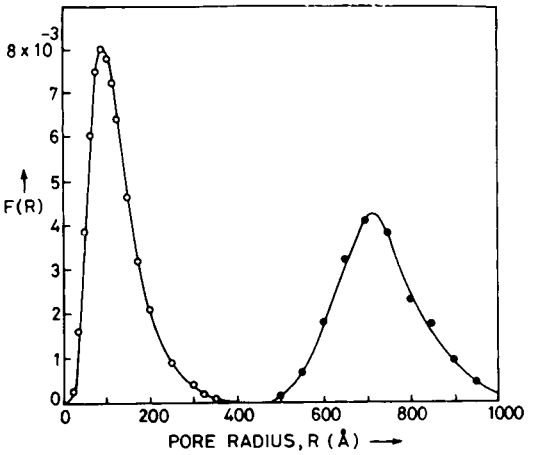

Fig. 4(b). Pore-size distribution in unoriented polyester: (○) As-spun Tow; (●) Tow tension-quenched at 200°C.

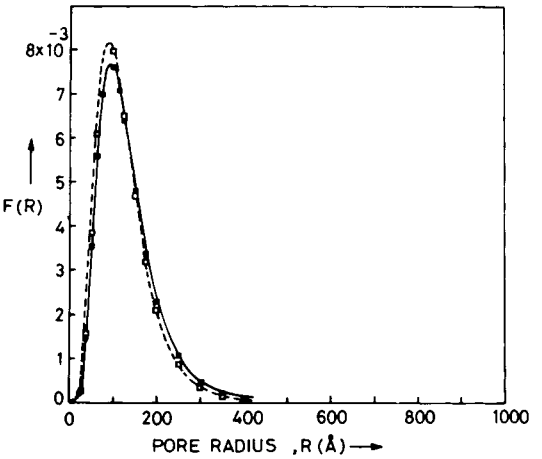

Fig. 4(c). Pore-size distribution in oriented polyester: (- - □ -) Drawn 400%; (■) Drawn 400%, Tension-quenched at 200%.

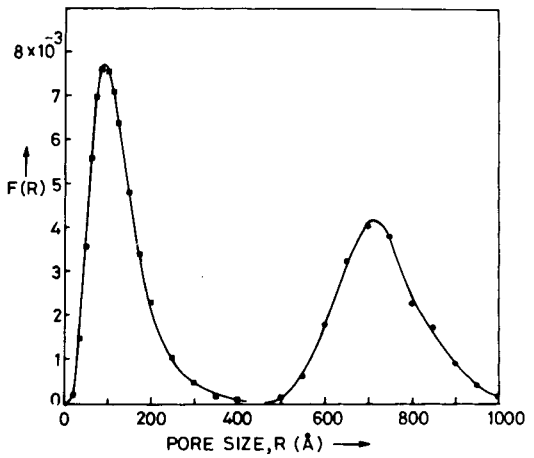

Fig. 4(d) Pore-size distribution in crystalline polyester: (- ● -) As-spun tow tension-quenched at 200°C; (- ■ -) Tow drawn 400%, tension-quenched at 200°C.

mation due to elongation during the cold-drawing process resulting only in a redistribution of the pores along the length without any changes in sizes or shapes. (ii) Isothermal crystallization of amorphous tow produces a drastic change in the pore size spectrum. The distribution becomes broader and shifts towards high values of pore radius [Fig. 4(b)]. Many small pores expand individually and also merge together to form larger pores. There is a concommitant increase in total pore content C (Table I) which can be explained in terms of increased space between crystallites[4] as a result of increase in crystallite size upon heat setting. Thus changes in crystallinity in the unoriented state have a pronounced influence on the pore size distribution in the fiber matrix. (iii) Isothermal crystallization of drawn tow causes a slight shift of the pore size spectrum towards higher pore radii [Fig. 4(c)]. This shift is also reflected in the increased values of R_E and P (Table I). Since the molecules in drawn tow are highly oriented to begin with, isothermal crystallization produces a highly compact, well-ordered crystalline structure, leaving slightly increased spaces between crystallites. Annealing reduces the volume fraction of pores[29] in this case (Table I). (iv) The pore size spectrum in crystallized unoriented tow and crystallized drawn tow are different [Fig. 4(d)] due to differences in their morphology (i.e., pore content) despite having a high degree of crystallinity which is a feature common to both samples. Thus initial orientation of the chains prior to crystallization during heat setting does have a profound influence on the pore size distribution perpendicular to the fiber axis after crystallization.

There is only one peculiar result listed in Table I which is worth mentioning. The specific surface S_{sp}, which represents the ratio of the total surface area S of the scattering material to the sample volume V, has the same value (0.06 m^2/cm^3) for samples 1–3, but has an appreciably lower magnitude of 0.025 m^2/cm^3 for sample 4 (crystallized drawn tow). This indicates a lower availability of surface area per unit volume of the scattering material, suggesting that a highly dense structure results when highly oriented material is crystallized under tension. Structural data obtained on various PET samples from density, birefringence, sonic modulus, X-ray diffraction, and infrared measurements along with values of dye uptake are given in Table II.

Dyeing and Morphological Parameters

Let us examine the DU values as a function of volume fraction of the noncrystalline regions. From Figure 5, it can be easily seen that the volume fraction of noncrystalline (or crystalline) regions does *not* show a consistent influence on the DU of PET fibers. The decrease in the total volume of noncrystalline regions by cold-drawing the undrawn amorphous fibers is only slight (Table II), but the dye uptake decreases considerably. On the other hand, despite a large decrease in the total volume of the noncrystalline regions, the undrawn heat set PET fibers show only slightly lower dye uptake than the undrawn as-spun fibers. It is also important to take note from Table II that the heat set undrawn fibers and heat set cold-drawn fibers possess almost the same volume fraction of noncrystalline regions but their DU values differ very considerably. From Figure 5, it can be

TABLE II
Comparison of Structural Parameters and Dye Uptake

No.	Sample particulars	X-ray crystallinity DC(%)	Density (g/cc)	Bire-fringence Δn	Sonic modulus E (g/den)	Total molecular orientation α	Relative "trans" content A_{975}/A_{1508}	Dye take DU (%)
1	amorphous tow	13	1.349	0.008	27.1	0.03	0.49	1.80
2	amorphous tow, cold drawn by 400%	19	1.365	0.196	100.1	0.74	0.86	0.70
3	amorphous tow TQ, 200°C	56	1.399	−ve	31.7	0.17	0.95	1.43
4	amorphous tow, cold drawn by 400%, TQ, 200°C	49	1.398	0.228	131.7	0.08	1.24	0.14

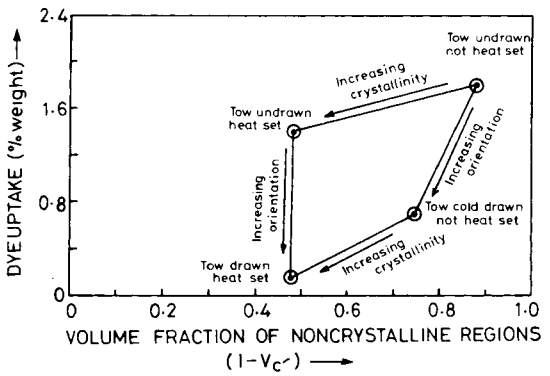

Fig. 5. Dye uptake as a function of the noncrystalline content.

inferred that the volume fraction of the noncrystalline regions has perhaps only a rather negligible influence as compared to the orientation of macromolecular chains (see also Table II). It is obvious from the foregoing discussion, as well as from published literature, that the dependence of dye uptake on crystallinity[1,3,5] or orientation is casual rather than causal. It is the changes in the pore structure of fibers, which may occasionally accompany or be produced by the changes in fiber morphology (orientation and crystallinity), that are responsible for the changes in dye uptake.

Dyeing and Fiber Porosity

In Table III, dye uptake values are listed along with those morphological parameters which have some bearing on DU by PET. Dye uptake or sample 4 is lowest among the four samples studied. It is also interesting to note that the specific surface, as well as pore content, has the lowest magnitude for this sample. Comparing the DU of sample 1 and sample 3, it is seen that sample 3 has only slightly lower DU than sample 1, despite an increase in X-ray DC from 13% to 56%! This is explained in terms of the considerably higher pore content in sample 3 (Table III) as well as increased pore sizes (Table I and Figs. 4). Comparing the dye uptake of sample 3 and sample 4, it is seen that the latter has a considerably lower DU than the former and both have more or less the same level of crystallinity. Again, this reduction in dye uptake can be correlated with the reduction both in the pore content as well as the specific surface (Table III). The correlation of dye uptake with fiber pore structure breaks down while comparing sample 1 with sample 2. In this particular case, one has to invoke the "tortuosity" concept[4,30] put forward by Warwicker[4] (two subsections below) to explain the lower dye uptake by the oriented sample.

Solvent Diffusion and Fiber Pore Structure

Data on critical dissolution time (CDT) measurements on PET samples has been incorporated in the last column of Table III, even though it does not have a direct correspondence with dye uptake. The reason for doing so is that the CDT data correlate well with the fibre pore structure parameters.

From Table III, it can be seen that samples 1, 2, and 3 have the same

TABLE III
Morphological Parameters Which Influence Dye Uptake by Polyester

No	Sample particulars	Dye uptake DU (%)	Pore content C(%)	X-ray crystallinity DC(%)	Specific surface S_{sp} (m^2/cm^3)	Total molecular orientation α	Relative "trans" content A_{975}/A_{1508}	$\log_{10}$(CDT)
1	amorphous tow	1.80	0.04	13	0.062	0.03	0.49	0.477
2	amorphous tow, cold drawn 400%	0.70	0.04	19	0.062	0.74	0.86	0.477
3	Undrawn tow, tension-quenches at 200°C	1.43	0.16	56	0.061	0.17	0.95	0.477
4	drawn tow, tension-quenched at 200°C	0.14	0.02	49	0.025	0.80	1.24	4.401

CDT values, despite their widely different morphological order as reflected by crystallinity and orientation. Apparently, the solvent molecules diffuse as easily in the highly oriented amorphous structure (sample 2) as in the unoriented amorphous structure (sample 1). Likewise, the rate of diffusion is same in the unoriented crystalline structure (sample 3) as well as in the unoriented amorphous structure (sample 1). This points out that the solvent diffusion behavior is not governed by orientation or the total value of non-crystalline regions.

The observed CDT results (Table III) are best explained in terms of fiber pore structure. Solvent molecules, being smaller than dyestuff molecules, can diffuse through the fiber structure much more easily (compared to dyes), since they require a much lower activation energy. However, there is a critical or minimum pore volume necessary for diffusion. If the pore volume is less than the critical value, solvent diffusion will not occur, or, if it occurs, it will take practically an infinitely long time. Dissolution of samples 1–3 occurs within 3 s, whereas the dissolution of sample 4 requires as much as 7 h! Again, looking at the pore structure data of sample 4 (Table III), it can be seen that this particular sample has the least pore content value of 0.02% and *also* the least value of specific surface. These two parameters are best correlated with the CDT data for all the four PET samples.

It appears, from this that, a more reasonable explanation of these results can only be given by assuming that, dye or solvent diffusion occurs into the pores or other microdefects in the fiber matrix as envisaged in Warwicker's model.[4] Thus the *total pore content and the tortuosity of the diffusion channels are the dominent controlling factors for the dye or solvent diffusion phenomenon.*

Proposed Structural Model for Explaining the Dye and Solvent Diffusion Behavior in Polyester

Figures 6 shows the network structural models proposed to explain the dye diffusion behavior of PET samples. Similar to Warwicker's concept,[4] the dye crystallites, or aggregates are assumed to be platelet or rod-shaped, which are embedded in a noncrystalline matrix. In the undrawn amorphous tow (sample 1), molecular chains in the noncrystalline regions are randomly oriented and diffusion channels (pores) are, therefore, tortuosity-free [Fig. 6(a)]. Upon cold-drawing the amorphous tow, the pore content remains the same (Table I), but the tortuosity increases owing to the large increase in the macromolecular orientation [Fig. 6(b)].

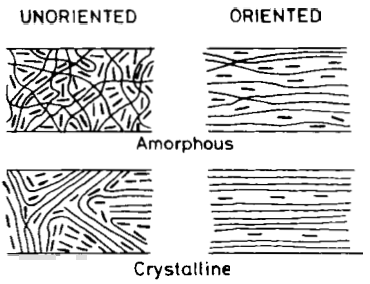

Fig. 6. Effect of chain/pore tortuosity on dye uptake.

Whether the tortuosity of the pores influences the diffusion behavior or not is dependent on the size of the diffusing molecule *relative* to the size of the pores. If the molecule is very small, the shape and tortuosity of the voids will have a negligible effect on the rate of diffusion. The rate of diffusion will then be dependent only on the total pore content. Because of their smaller sizes, many solvent molecules diffuse with the same rate in both unoriented amorphous and highly oriented amorphous polyester fibers, whereas some of the larger-sized disperse dye molecules at lower dyeing temperatures, or in the absence of carriers, find it difficult to penetrate with ease in the highly oriented fiber matrix as the tortuosity of the pore space increases considerably with increasing molecular orientation. As the total pore content may not have been altered by orientational drawing, the large reduction in dye uptake must be due to the large increase in the tortuosity of the pores or closer organized packing of the polyester chains.

In the case of unoriented crystalline fibers [Fig. 6(c)] the total pore content may not have changed, or only increased slightly, so that, in spite of the large reduction in the volume of the noncrystalline regions, the dye uptake is only marginally affected by increased crystallinity. The solvent diffusion rate is therefore also unaffected.

In the highly oriented crystalline fibers [Fig. 6(d)], a decrease in pore content, as well as an increase in tortuosity, occurs, resulting in reduced dye and solvent molecule diffusion rates. This sample shows the lowest dye uptake and a very long critical dissolution time in phenol/TCE solution.

Figure 7 shows a photograph of dyed fibers pressed into the form of pellets for samples 1–4. The amount of dye picked up by the fibers appears to be in conformity with the schematic network models shown in Figure 6.

Figure 8 shows the corresponding wide-angle X-ray photographs for the same four samples and clearly brings out the nature and extent of crystallinity (3D order), as well as molecular chain orientation along the fiber axis for the four different samples.

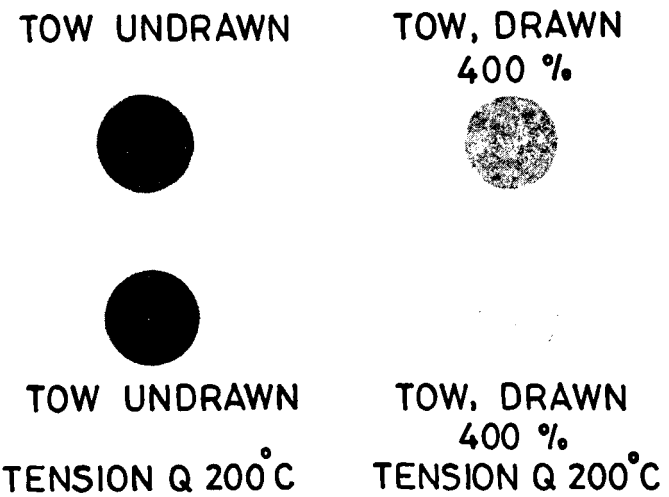

Fig. 7. Photograph of dyed pellets showing the extent of dye uptake.

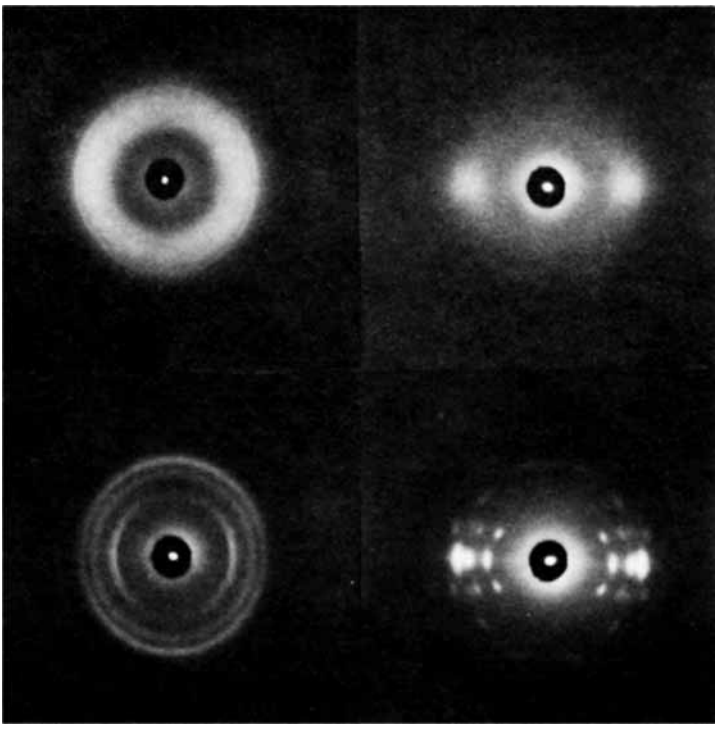

Fig. 8. Wide-angle X-ray photographs of polyester: (a) undrawn tow; (b) tow drawn to 400% extension; (c) undrawn, crystallized tow; (d) highly oriented and crystalline fibers (fiber axis vertical in all cases).

To conclude, it can be said that diffusion phenomena, whether of a solvent or a dye molecule, are controlled by the amount, size, and tortuosity of the pores in the matrix. The structural parameters, such as crystallinity or orientation, will have an influence on the diffusion behavior only when they affect the total pore content (volume), size, and/or the tortuosity of the diffusion paths.

If the material is highly oriented prior to setting, the ensuing crystallization on thermal treatment leads to highly oriented crystalline, as well as amorphous regions. This results in a closely packed structure with minimum pore space and high tortuosity of pores or channels. If the materials is only poorly oriented prior to heat setting, the ensuing crystallization after thermal treatment leads to either completely disoriented crystalline and noncrystalline regions or slightly perpendicularly oriented crystalline regions. This gives rise to a loosely packed structure with as much, or sometimes more, pore space and less tortuosity. This is more clearly illustrated in Figures 9(a) and 9(b) which are the models of fine structure suggested by the authors for the explanation of thermal crystallization of polyester having an initially oriented or unoriented fibrous structure respectively. It will be easier now to understand why these two fibrous materials show enormous differences in dye uptake, while they possess roughly the same volume fraction of crystalline regions in the matrix.

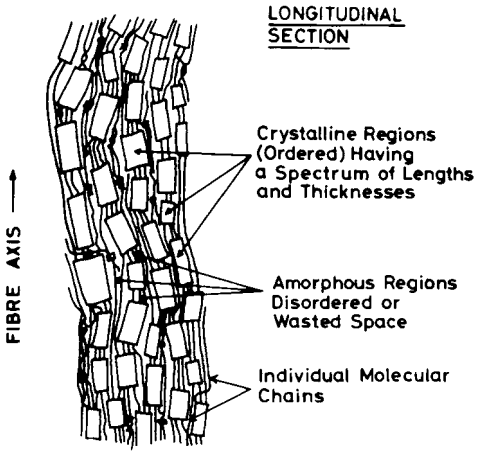

Fig. 9a. Model showing crystallization in an initially ordered or oriented sample.

CONCLUDING REMARKS

Although the significance of fiber pore structure in diffusion-controlled processes (solvent swelling, dye uptake) was well-known, the methods for its quantitative characterization have rarely been used. The present work, employing SAXS for the characterization of internal surface and pore size spectrum in PET, fulfills this need and also the need for a quantitative characterization of the noncrystalline domains within the fiber. It attempts to offer an explanation of polyester dyeing in terms of fiber porosity.

The scope of the present work is limited by the resolution of the Kratky SAXS apparatus (1000 Å in our case), which means that the distribution of pore radii has been studied only in the range between 25 and 1000 Å. The resolution of the apparatus can be improved by employing narrower slits, but this does not help because the intensities become so low that they

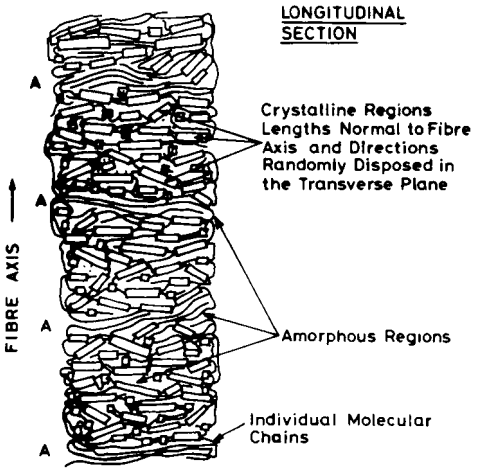

Fig. 9(b). Model showing crystallization in an initially disordered or unoriented sample.

cannot be accurately measured. The SAXS results may also throw some light on pore channel tortuosity (i.e., the anisotropy of pore shape), but it was beyond the scope of the present work and may be worthy of future sophisticated investigations using the SAXS technique employing powerful X-ray sources (e.g., rotating-anode X-ray generator) and simultaneous detection over the entire range of the scattering curve (by means of a position sensitive detector).

When one looks at the dimensions of dye molecules (let alone aggregates of such), one then requires very substantial pore volumes and work associated with their creation to accomodate such diffusing species. This makes it improbable[2] that anything other than monomolecular species are involved in such diffusion processes with disperse dyes in PET substrate. How many molecules of absorbed dye of a particular constitution can be accommodated within pores and on the internal surfaces of fibers before saturation DU is achieved cannot yet be determined. But it is research of this kind, together with a greater knowledge and understanding about pore shapes, sizes, and distributions, strengths of valence forces, and molecular stacking characteristics of dyes, which may ultimately help to answer such questions. As Warwicker[4] points out, the dye itself is a platelike molecule and probably penetrates the pore structure edge-on, so that the width of pores need not be great (~5 Å) and might be enlarged to some extent by the dye itself. SAXS studies of dyed PET fiber should also be attempted in future investigations.

The authors wish to thank Dr. T. Radhakrishnan, Director of ATIRA, for permission to publish this work. One of them (M.V.S. Rao) is also grateful to the Council of Scientific and Industrial Research, India, for financial assistance in the form of a Junior Research Fellowship.

References

1. G. Valk, G. Jellinek, and U. Schroder, *Tex. Res. J.*, **50**, 46 (1980).
2. W. McDowell, *Text. Chem. Colour.*, **10**, 131 (1978).
3. R. S. Asquith, *Text. Recorder*, **80** (Mar), 58 (1963).
4. J. O. Warwicker, *J. Soc. Dyers Colour.*, **88**, 142 (1972).
5. J. H. Dumbleton, J. P. Bell, and T. Murayama, *J. Appl. Polym. Sci.*, **12**, 2491 (1968).
6. G. Porod, *Kolloid Z.*, **124**, 83 (1951).
7. G. Porod, *Kolloid Z.*, **125**, 51 (1952).
8. G. Porod, *Kolloid Z.*, **133**, 16 (1953).
9. G. Porod, *Makromol. Chem.*, **35**, 1 (1960).
10. O. Kratky and G. Miholic, *J. Polym. Sci.*, **C2**, 449 (1963).
11. T. Ratho and H. Patel, *J. Phys., D* **14**, 2169 (1981).
12. A. Patel *et al.*, *Chem. Abstr.*, **92**, 182422 (1980).
13. T. Misra, A. Patel, and J. Patnaik, *J. Polym. Sci. Chem.*, **18**, 1359 (1980).
14. T. Misra, K. C. Patra, and T. Patel, *J. Polym. Sci. Chem.*, **19**, 3165 (1981).
15. T. Ratho and T. Misra, *J. Polym. Sci., A-1*, **9**, 3491 (1971).
16. M. G. Dobb and D. J. Johnson, *Polymer*, **20**, 1284 (1979).
17. I. Tomizuka and D. J. Johnson, *Yogyo Kyokai Shi*, **86**, 186 (1978).
18. C. G. Vonk and G. Korleve, *Koll. Z. Z. Polym.*, **220**, 19 (1967).
19. J. Andriessen and J. Van Soest, *Text. Verdlung*, **3**, 618 (1968).
20. V. Baumgarye, *Melliand Textilber.*, **53**, 790 (1972).
21. G. Galil, *Text. Res. J.*, **43**, 615 (1973).
22. R. J. Samuels, *Structural Polymer Properties*, Wiley, New York, 1974.
23. I. M. Ward, *Structure and Properties of Oriented Polymers*, Applied Science, London, 1975.

24. A. Guinier and G. Fournet, *Small-Angle Scattering of X-Rays*, Wiley, New York, 1955.
25. O. Kratky, *Pure Appl. Chem.*, **12**, 483 (1966).
26. P. Mittelbach and C. Porod, *Kolloid Z. Z. Polym.*, **202**, 40 (1965).
27. S. D. Harkness, R. Gould, and J. J. Hren, *Phil. Mag.*, **19**, 115 (1969).
28. G. F. Neilson, *J. Appl. Crystallogr.*, **6**, 386 (1973).
29. W. O. Stratton, *J. Polym. Sci.*, **22**, 385 (1956).
30. J. J. Donze, G. Bouchet, R. Freytag, J. Chabert, R. Schneider, and P. Viallier. *J. Soc. Dyers Colour.*, **91**, 336 (1975).

Received May 24, 1983
Accepted January 4, 1985